

A suite of coupled model test cases

Stephen.Griffies@noaa.gov
 NOAA/GFDL
 Princeton, USA
 May 14, 2012

Abstract

This document presents a suite of MOM test cases that use MOM as a component in a coupled model, including coupled ocean-sea ice models. These tests are generally realistic and are taken from published configurations.

Contents

1	General comments on the test cases	1
2	CORE Normal Year Forcing experiments	2
3	Global ocean-ice-biogeochemistry model	24
4	Global coupled model CM2.1	24
5	Global coupled earth system model ESM2M	24

1 General comments on the test cases

Test cases in this document are offered as a means to explore various numerical and physical options, thus allowing the user to verify that the code is performing in a manner consistent with that at GFDL. This form of verification is critical as one adopts the code for his or her particular research purposes. The test cases also provide a sense for some of the options available in the code, though by no means are all options exercised in the test cases. Finally, these tests have been taken from realistic configurations that have generally been part of a publication. Consequently, they may form the basis for future research.

1.1 Regression Testing for Computational Integrity

Output from the test cases provided with the MOM distribution is based on short integrations that verify the computational integrity of a simulation. The associated runscripts are provided that allow the user to rerun the regressions. These *regression test suites* (RTS) aim to verify that the following identities hold, with precision maintained to all computational bits:

- Stopping and then restarting the integration will not change answers. That is, we insist on the identity

$$X \text{ day integration} = X/2 \text{ day integration} + X/2 \text{ day integration}. \quad (1)$$

This test verifies that all the relevant fields are properly stored in the restart files, and that no spurious reinitialization step is performed during the beginning of the second leg.

- Changing the number of computer processors will not change the answers. This test examines whether the code is properly written for parallel machines. Its satisfaction requires that all message passing be correctly performed so that accessed halo points are filled with their proper values. In the early days of parallel computing with MOM, this test was very tedious to satisfy, since our experience was based on serial computing. Now, after some years of experience, it is generally straightforward to code in a manner that ensures answers do not change when processor counts change.

Satisfaction of these two tests is critical to maintain computational integrity of the code.

It is important to note that the runscripts for the regressions are distributed with the following settings:

- `diag_step` is set to a small number, such as 1 or 12, in various diagnostic modules. This setting means that various numerical diagnostics are run at a very high frequency. These diagnostics can be expensive. It is therefore strongly recommended that the setting for `diag_step` be increased to a much larger number when running experiments for long periods of simulation time. Otherwise, the model will be unreasonably slow.
- The diagnostic tables are setup to output netCDF diagnostics at a very high frequency, such as daily. Again, this high frequency is unreasonable when running simulations for long periods of time. The output produced will be enormous, and the model will run at a much slower pace. Additionally, a large number of diagnostics are included in the `diag_table`, many of which may not be of interest to the user. Therefore, prior running an experiment, it is important to edit the `diag_table` to refine the desired output.

1.2 Perspectives on the test cases

The material in this document provides a rough guide to the various ocean-coupled test cases. We present a sprinkling of model output to allow interested users to run simulations at their institution to verify that the code has been properly ported. Many details of the experiments are omitted, with examination of the supplied runscripts providing more details. Furthermore, a full accounting of the test cases, both their design and simulation characteristics, is beyond the scope of this document. Indeed, a full discussion would constitute a research paper. We thus present a taste, with further details readily found by diving into the model, running experiments, and performing analysis.

Some test cases are based on research experiments conducted at GFDL and elsewhere. They may thus serve as useful starting points for research using MOM. It is nonetheless critical that the user *not* blindly assume that a test case is precisely appropriate for a particular research project. Instead, one is strongly encouraged to scrutinize each option in a test case before concluding that it is relevant.

As there are many options in MOM, it is not feasible to exercise all options with only a few test cases. Hence, some tests are distributed with more options enabled than scientifically appropriate. Conversely, many options are not fully exemplified by the test cases. Omitted options include the *experimental* options sprinkled through MOM, with these options *not* supported for general use. The developers are aware of the limitations in the test cases, but choose to release the incomplete suite of tests in hopes that *something* is preferable to *nothing*.

2 CORE Normal Year Forcing experiments

MOM comes with global ocean-ice test cases that are forced with the Normal Year Forcing dataset from [Large and Yeager \(2004\)](#), along with updates to the river forcing based on the seasonally varying [Dai et al. \(2009\)](#) dataset. The experimental design follows the Coordinated Ocean-ice Reference Experiments Normal Year Forcing protocol (CORE-NYF) as detailed in [Griffies et al. \(2009\)](#). The purpose of this section is to summarize salient features of this experiment as implemented in the MOM code release from 2012, and to exhibit sample analyses from the model configurations with MOM coupled to the GFDL Sea Ice Simulator (SIS) code.

Three CORE-NYF test cases released with MOM are based on ocean-ice components taken from three fully coupled climate and earth system models with nominally one-degree horizontal grid spacing. The fourth model discussed in this chapter is the MOM4.0 version of the CORE/CM2.1 simulation, which was the MOM-contribution to the [Griffies et al. \(2009\)](#) paper. These models are listed in Table 1, with the remainder of this chapter detailing the model configurations and providing sample results.

Caveat

For those interested in running CORE simulations using either the GFDL model configuration, or their own, it is strongly advised that one download the CORE forcing directly from the CORE web site at

<http://data1.gfdl.noaa.gov/nomads/forms/mom4.html>

since the CORE dataset is updated more frequently than that MOM code distribution. Indeed, the CORE-NYF released with the December 2011 MOM4p1 still uses the original version of the CORE-NYF dataset from Large and Yeager (2004), rather than the updated version from Large and Yeager (2009).

EXPERIMENT NAME	DOCUMENTATION	SECTION
CORE/CM2.1old	Griffies et al. (2005)	2.1.2
CORE/CM2.1new	Griffies et al. (2005)	2.1.2
CORE/ESM2M	Dunne et al. (2012a)	2.1.3
CORE/ESM2Mb	NA	2.1.4

Table 1: Global ocean-ice CORE-NYF experiments described in this chapter.

2.1 The ocean and sea ice configurations

This section provides details for the ocean and sea ice configurations used in the three CORE-NYF simulations.

2.1.1 Vertical coordinate

MOM generalizes the vertical discretization of its levels. We chose for the CORE-NYF ocean-ice configurations the z^* vertical coordinate of Stacey et al. (1995) and Adcroft and Campin (2004), defined according to

$$z^* = H \left(\frac{z - \eta}{H + \eta} \right). \quad (2)$$

In this equation, $z = \eta(x, y, t)$ is the deviation of the ocean free surface from a state of rest at $z = 0$, and $z = -H(x, y)$ is the ocean bottom. Whereas a geopotential ocean model places all free surface undulations into the top model grid cell, a z^* model distributes the undulations throughout the ocean column. All grid cells thus have a time dependent thickness with z^* . Surfaces of constant z^* differ from geopotential surfaces according to the ratio η/H , which is generally quite small. Hence, surfaces of constant z^* are quasi-horizontal, thus minimizing difficulties of accurately computing the horizontal pressure gradient (see Griffies et al., 2000, for a review). The z^* vertical coordinate is analogous to the “eta” coordinate sometimes used for atmospheric models (Black, 1994).

We chose z^* because of its enhanced flexibility when considering two key applications of climate models beyond those considered in this paper. The first application concerns large surface height deviations associated with tides and/or increased loading from sea ice (e.g., a global cooling simulation). The z^* model allows for the free surface to fluctuate to values as large as the local ocean depth, $|\eta| < H$, whereas the geopotential model is subject to the more stringent constraint $|\eta| < \Delta z_1$, with Δz_1 the thickness of the top grid cell with a resting ocean. The ocean models configured here set a minimum depth to $H \geq 40\text{m}$, whereas $\Delta z_1 = 10\text{m}$ (note that there is no *wetting and drying* algorithm in MOM4p1). This flexibility with z^* is further exploited if considering even finer vertical grid resolution. The second application where z^* is useful concerns increased land ice melt that adds substantially to the sea level, as in the idealized studies of Stouffer et al. (2006b), Kopp et al. (2010), and Yin et al. (2010). Placing all of the surface expansion into the top model grid cell, as with the free surface geopotential model, greatly coarsens the vertical grid resolution in this important portion of the ocean, whereas the z^* model does not suffer from this problem since the expansion is distributed throughout the column.

2.1.2 CORE/CM2.1old and CORE/CM2.1new

The CM2.1 coupled climate model was developed at GFDL for the IPCC AR4 assessment, and is documented by Griffies et al. (2005), Gnanadesikan et al. (2006), Delworth et al. (2006), Wittenberg et al.

(2006), and Stouffer et al. (2006a). The full climate model, using the geopotential vertical coordinate. The MOM contribution to the Griffies et al. (2009) paper is based on the ocean-ice configuration from CM2.1, using the MOM4.0 code base. The more recent MOM version of CM2.1-CORE compares to that in Griffies et al. (2009) in the following ways.

- PHYSICAL PARAMETERIZATIONS: All physical parameterizations are the same for both the MOM4.0 version in Griffies et al. (2009) and MOM5 version.
- VERTICAL COORDINATE
 - CM2.1-CORE in Griffies et al. (2009) uses the geopotential coordinate available in MOM4.0.
 - CM2.1-CORE from MOM5 uses the z^* vertical coordinate defined by equation (2)
- NORMAL YEAR FORCING
 - CM2.1-CORE from MOM4.0 in Griffies et al. (2009) uses the Large and Yeager (2004) normal year forcing.
 - CM2.1-CORE from MOM5 also uses the normal year forcing from Large and Yeager (2004).
- RIVER RUNOFF
 - CM2.1-CORE from MOM4.0 in Griffies et al. (2009) uses the annual mean river runoff from Large and Yeager (2004), with this runoff spread rather widely from river mouths as in Figure
 - CM2.1-CORE from MOM5 uses the seasonally varying river runoff dataset from Dai et al. (2009), with this runoff inserted into the ocean in a very modestly diffused manner to avoid single-grid point insertions. The wide spreading used in Large and Yeager (2004) is avoided.
- SALINITY/WATER RESTORING: PART I
 - CM2.1-CORE from MOM4.0 in Griffies et al. (2009) converted the surface salinity restoring to a water flux, with a net zero water flux exchanged across the ocean from this restoring term.
 - CM2.1-CORE from MOM5 keeps the salinity restoring as a salt flux, with the net salt added to the ocean kept at zero for each time step.
- SALINITY/WATER RESTORING: PART II
 - CM2.1-CORE from MOM4.0 in Griffies et al. (2009) used 300 days over 50m as a piston velocity for the the salinity restoring.
 - CM2.1-CORE from MOM5 also uses 300 days over 50m as a piston velocity. Additionally, the mismatch between model and climatological sea surface salinity, $\Delta(SSS)$, is limited to

$$|\Delta(SSS)| < 0.5 \text{ ppt} \quad (3)$$

in the computation of the surface salinity relaxation. This limit avoids extreme relaxation fluxes that may occur, for example, in the vicinity of the western boundary currents that are generally not realistically represented in coarse OGCMs. If too much fresh water is added due to large biases in the western boundary current, then this potentially large amount of fresh water will be transported poleward, which will spuriously weaken the Atlantic overturning circulation. A summary of this unstable feedback is given in Griffies et al. (2009).

- SALINITY/WATER RESTORING: PART III: The salinity restoring field has been updated relative to the original field used in Griffies et al. (2009), to correct a few biases and problem areas. See the CORE web site <http://data1.gfdl.noaa.gov/nomads/forms/mom4/COREv2.html> for details.

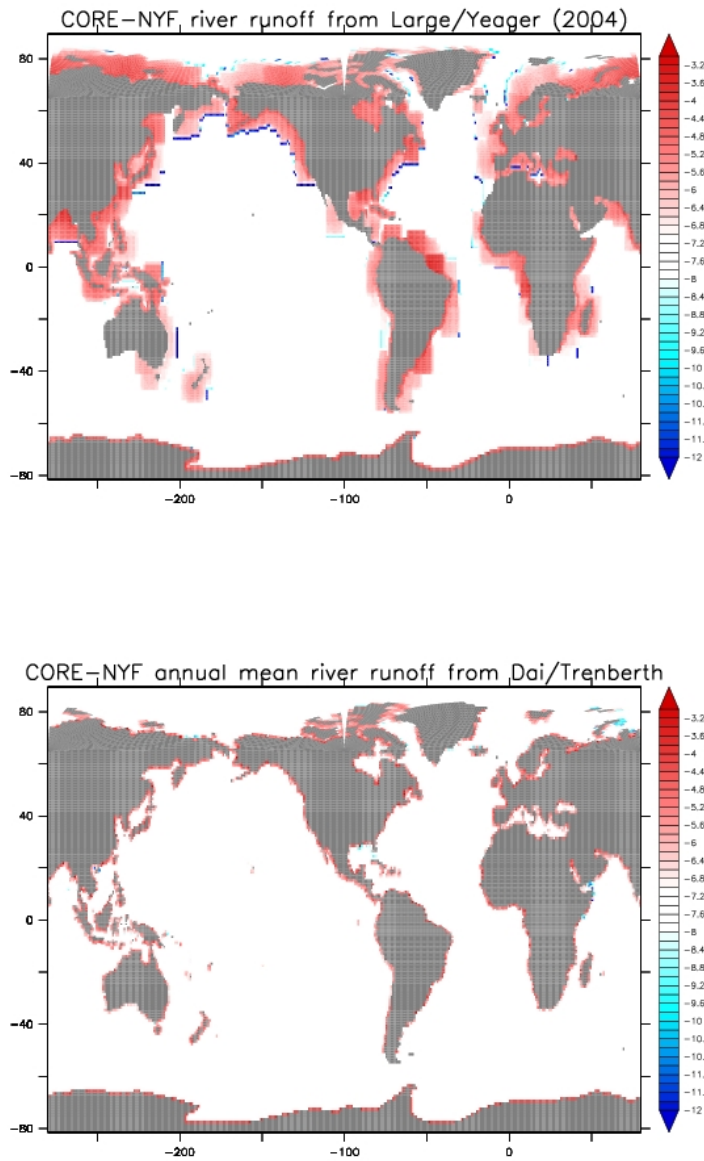


Figure 1: Shown here is the log of the river runoff mass fluxes ($\text{kg m}^{-2} \text{s}^{-1}$) used for the [Large and Yeager \(2004\)](#) and the annual mean of the repeating annual cycle of [Dai et al. \(2009\)](#) as used in the CORE-NYF simulations detailed in this chapter. Note the absence of *a priori* river spreading of runoff fluxes for the [Dai et al. \(2009\)](#) data. In fact, there is a slight amount of spreading applied according to a Laplacian operator, but that spreading is very small relative to that used in the original [Large and Yeager \(2004\)](#) approach. The global net mass flux into the ocean from the [Large and Yeager \(2004\)](#) runoff is $1.24 \times 10^9 \text{ kg s}^{-1}$, whereas the annual mean from [Dai et al. \(2009\)](#) is $1.22 \times 10^9 \text{ kg s}^{-1}$.

2.1.3 CORE/ESM2M

ESM2M is an earth system model developed at GFDL for the IPCC AR5 assessment, and it is documented by [Dunne et al. \(2012a\)](#). The ocean component of ESM2M is configured with the same horizontal and vertical grid dimensions as the CM2.1 ocean component. Both the ESM2M and CM2.1 configurations released as part of the CORE-NYF simulations use the rescaled geopotential coordinate z^* as defined in Section 2.1.1. Additional differences between the ocean and sea ice components include the following.

- **TRACER ADVECTION:** ESM2M uses the multi-dimensional piecewise parabolic method (MDPPM) ported from the MITgcm ([Marshall et al., 1997](#)). In idealized simulations, the MDPPM method was found to be more accurate (less diffusive) than the CM2.1 advection scheme while still preserving monotonicity.
- **NEUTRAL DIFFUSION:** Neutral in both models is based on [Griffies et al. \(1998\)](#), with a constant diffusivity of $600\text{m}^2 \text{s}^{-1}$ and the hyperbolic tangent slope tapering scheme of [Danabasoglu and McWilliams \(1995\)](#).
 - CM2.1 uses a maximum slope of 1/500.
 - ESM2M uses a maximum slope of 1/200.
- **MESOSCALE EDDY INDUCED ADVECTION:**
 - CM2.1 uses the skew fluxes of [Griffies \(1998\)](#) to implement the [Gent et al. \(1995\)](#) scheme. The eddy diffusivity is flow dependent yet depth independent, with the algorithm detailed in [Griffies et al. \(2005\)](#). The diffusivity is kept within a range of $100\text{m}^2 \text{s}^{-1} -- 600\text{m}^2 \text{s}^{-1}$. A linear scaling of the quasi-Stokes streamfunction in regions where either the neutral slope is greater than 1/500, or within the planetary boundary layer.
 - ESM2M computes the quasi-Stokes streamfunction via a boundary value problem extending across the full column after [Ferrari et al. \(2010\)](#), which contrasts with the local approach of [Gent and McWilliams \(1990\)](#) and [Gent et al. \(1995\)](#). The maximum slope parameter is no longer relevant for calculation of the quasi-Stokes streamfunction using the [Ferrari et al. \(2010\)](#) approach. The diffusivity is allowed to vary over the slightly larger range of $100\text{m}^2 \text{s}^{-1} -- 800\text{m}^2 \text{s}^{-1}$ rather than the $100\text{m}^2 \text{s}^{-1} -- 600\text{m}^2 \text{s}^{-1}$ used in CM2.1.
- **KPP BOUNDARY LAYER SCHEME:** ESM2M updates the K-profile parameterization [Large et al. \(1994\)](#) based on [Danabasoglu et al. \(2006\)](#).
- **CHLOROPHYLL FOR SHORTWAVE ATTENUATION:**
 - CM2.1 uses the chlorophyll dataset prepared by [Sweeney et al. \(2005\)](#) for use in attenuating shortwave radiation into the upper ocean, based on the optics scheme of [Morel and Antoine \(1994\)](#). An arbitrary maximum depth of 100m is set, below which zero radiation penetrates.
 - ESM2M prepared an updated chlorophyll dataset based on the longer available SeaWiFS satellite product. It also attenuates optics based on the optics scheme of [Manizza et al. \(2005\)](#). An arbitrary maximum depth of 200m is set, below which zero radiation penetrates.
- **SUBMESOSCALE PARAMETERIZATION SCHEME:** CM2.1 did not use a parameterization of the upper ocean restratification effects from submesoscale eddies. In contrast, ESM2M used the scheme of [Fox-Kemper et al. \(2008\)](#) as implemented according to [Fox-Kemper et al. \(2011\)](#).
- **INTERNAL TIDE INDUCED MIXING:**
 - CM2.1 used the time independent, depth dependent vertical diffusivity profile of [Bryan and Lewis \(1979\)](#), but with smaller overall diffusivities than those of the original [Bryan and Lewis \(1979\)](#) paper.
 - ESM2M employs the [Simmons et al. \(2004\)](#) internal tide mixing parameterization, along with a depth independent background diffusivity of $1 \times 10^{-5} \text{ m}^2 \text{s}^{-1}$ in the tropics and $1.5 \times 10^{-5} \text{ m}^2 \text{s}^{-1}$ poleward of $30^\circ 30$ latitude.

- CONVECTIVE ADJUSTMENT:

- In the presence of vertically unstable water columns, CM2.1 introduced a large diffusivity as well as the [Rahmstorf \(1993\)](#) convective adjustment scheme. The CM2.1 implementation of [Gent et al. \(1995\)](#) had a limitation whereby it was only valid in regions satisfying $N^2 \geq 0$. This limitation in turn necessitated the use of the [Rahmstorf \(1993\)](#) scheme, since this convective adjustment scheme ensures that the vertical profile exhibits no regions with $N^2 < 0$.
- The ESM2M implementation of [Ferrari et al. \(2010\)](#) allows for $N^2 < 0$, and so the [Rahmstorf \(1993\)](#) scheme was removed.

- HORIZONTAL FRICTION

- CM2.1 uses the horizontal anisotropic Laplacian friction scheme from [Large et al. \(2001\)](#) in the tropics, and an isotropic Laplacian scheme in the higher latitudes along with a Smagorinsky coefficient ([Griffies and Hallberg, 2000](#)).
- ESM2M uses an isotropic Laplacian friction and a western boundary enhanced biharmonic friction. Overall ESM2M has less frictional dissipation, which allows for more vigorous tropical instability wave activity. There is, however, a somewhat enhanced level of zonal grid noise in the tropics.

- GEOTHERMAL HEATING: ESM2M implements geothermal heating following from the approach of [Adcroft et al. \(2001\)](#), whereas CM2.1 does not have geothermal heating.

- SEA ICE

The ESM2M sea ice code is identical to that used for CM2.1, as documented in [Delworth et al. \(2006\)](#) and [Winton \(2000\)](#), and it uses the same horizontal grid arrangement of the ocean model. However, the ice and snow-on-ice albedos have been tuned brighter in ESM2M relative to the CM2.1 settings (see Table 2), which brings the ESM2M values to more realistic values based on the observations from ([Perovich et al., 2002](#)). ESM2M also uses the same snow-on-ice albedos as the CM3 coupled model documented by [Griffies et al. \(2011\)](#), but slightly different ice albedos.

PARAMETER	CM2.1	ESM2M	ESM2Mb
Snow albedo (dry/wet)	0.80/0.68	0.85/0.73	0.85/0.73
Ice albedo (dry/wet)	0.58/0.51	0.65/0.575	0.65/0.575
transition ΔT (Kelvin) from dry to wet	10	1	1

Table 2: Albedos used in the sea ice model for CM2.1 and ESM2M. The transition from dry to wet albedos occurs linearly, starting at 10K below freezing for CM2.1 and 1K below freezing for ESM2M. This transition range was a much larger (and less realistic) in CM2.1 to counteract biases that rendered too much Northern Hemisphere sea ice in CM2.1, especially in the North Pacific. The albedos in CM2.1 were similarly set low to reduce the excessive ice cover.

2.1.4 CORE/ESM2Mb

The earth system model ESM2Mb is an updated version of ESM2M, incorporating some bug fixes and some physical parameterization modifications. For the ocean, we identify the following changes that are relevant for the CORE-NYF test case in MOM.

- EDDY DIFFUSIVITY FOR PARAMETERIZED MESOSCALE EDDY ADVECTION

- ESM2M uses the range $100 \text{ m}^2 \text{ s}^{-1}$ to $800 \text{ m}^2 \text{ s}^{-1}$.
- ESM2Mb uses the range $100 \text{ m}^2 \text{ s}^{-1}$ to $1200 \text{ m}^2 \text{ s}^{-1}$.

We are motivated to extend the range given the studies of [Farneti et al. \(2010\)](#) and [Farneti and Gent \(2011\)](#) that indicate a wider range is necessary to more adequately respond to changes in zonal wind stress in the Southern Ocean.

- COASTAL TIDE MIXING SCHEME

The scheme from [Lee et al. \(2006\)](#) in principle should not impact regions away from the continental shelves. However, as implemented in both CM2.1 and ESM2M, this scheme has a bug that impacts the value of the diffusivity in deep ocean regions. In particular, the code was improperly implemented, so that the scheme could produce nontrivial diffusivities even in the deep ocean and reaching up through the pycnocline. This problem is largely hidden in CM2.1 due to the rather large background diffusivity chosen from the [Bryan and Lewis \(1979\)](#) scheme. However, for ESM2M, which used a much smaller background diffusivity, it is clear that the spurious feature from the [Lee et al. \(2006\)](#) scheme is unacceptable. We resolve this problem in ESM2Mb by modifying the [Lee et al. \(2006\)](#) scheme so that it is removed in non-shelf regions. Furthermore, an exponential decrease from the bottom upwards.

- BACKGROUND DIFFUSIVITY BASED ON MINIMUM DISSIPATION:

ESM2Mb specifies the background vertical diffusivity based on a minimum dissipation, which contrasts to the spatially constant background used in ESM2M. The use of a dissipation-based background is motivated by the approach taken in the ESM2G earth system model, which uses the isopycnal ocean GOLD (see [Dunne et al., 2012a](#), for more details of ESM2G).

2.1.5 Sample results

We have run the three CORE-NYF simulations for more than 500 years each. In this section, we present a suite of results from these simulations. We also compare to the CORE/CM2.1old simulation used in the [Griffies et al. \(2009\)](#) paper, which is based on the geopotential configuration in MOM4.0. This simulation is referred to here as CORE/CM2.1old, whereas the recent MOM5 simulation is COREnyf/CM2.1new. Notably, we are not prepared to provide a full discussion/analysis of the results presented here. We merely present the results as a brief atlas for comparison with the [Griffies et al. \(2009\)](#) results.

2.2 Horizontally averaged biases as a function of time

An interesting facet of the CORE-NYF simulations concerns the spin-up of the simulations. In Figures 2 and 3, we exhibit the horizontally averaged deviation of the temperature and salinity from the initial conditions, as a function of time. This diagnostic is quite valuable for measuring how much heat and salt is moved around in the ocean as a function of depth.

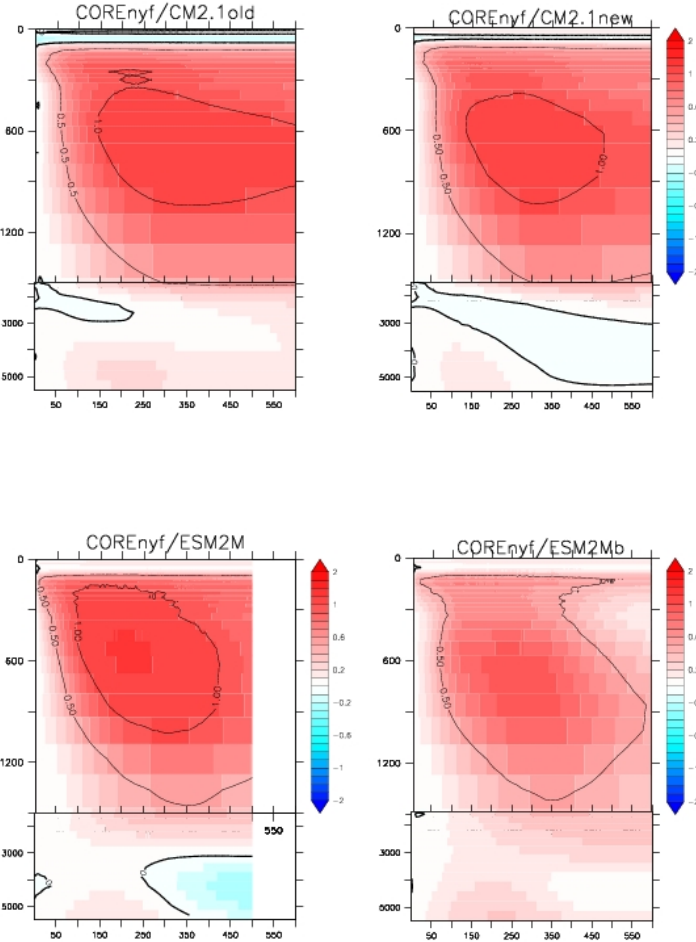


Figure 2: Globally averaged drift of the annual mean temperature (degrees C) as a function of depth (metres on vertical axis) and time (years on horizontal axis). This drift is defined as $T_{\text{drift}}(z, t) = (\sum_{xy} dx dy dz (T_{\text{model}} - T_{\text{initial}}^{\text{ann}})) / (\sum_{xy} dx dy dz)$, where $T_{\text{initial}}^{\text{ann}}$ is the annual mean from [Conkright et al. \(2002\)](#) and [Steele et al. \(2001\)](#), and \sum_{xy} is a horizontal sum. The upper 1500m is expanded relative to the deeper ocean, in order to highlight the generally larger surface drifts. 0.5°C contours are drawn to better gauge the magnitude of the drift. Note the generally smaller drift in the ESM2Mb simulation relative to the others. Compare to Figure 5 of [Griffies et al. \(2009\)](#) for results from other CORE-NYF simulations.

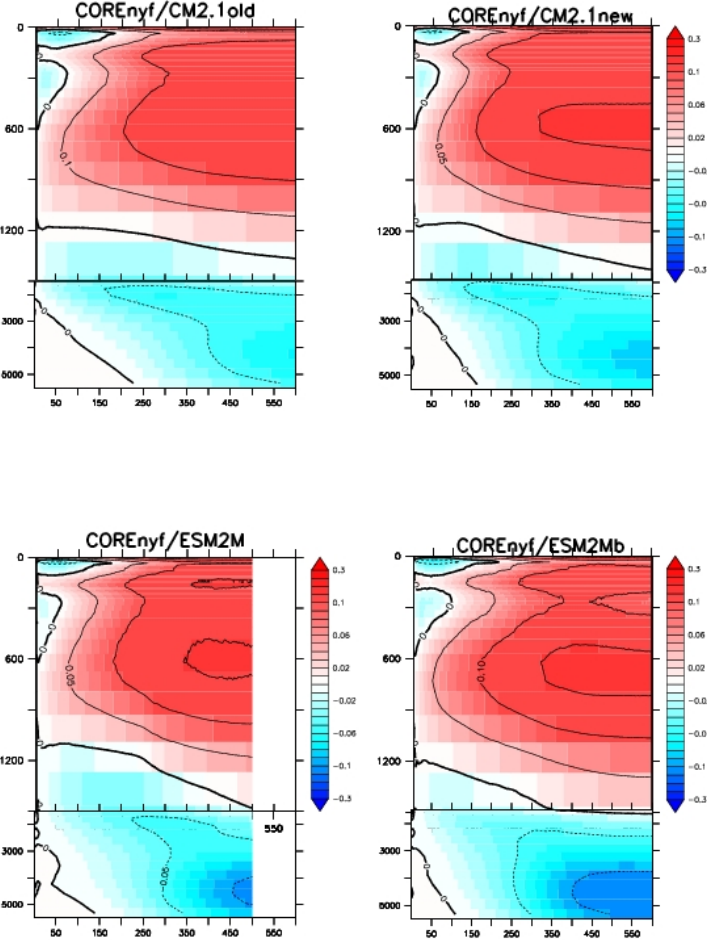


Figure 3: Globally averaged drift of the annual mean salinity (psu) as a function of depth (metres on vertical axis) and time (years on horizontal axis). This drift is defined as $S_{\text{drift}}(z, t) = (\sum_{xy} dx dy dz (S_{\text{model}} - S_{\text{initial}}^{\text{ann}})) / (\sum_{xy} dx dy dz)$, where $S_{\text{initial}}^{\text{ann}}$ is the annual mean from [Conkright et al. \(2002\)](#) and [Steele et al. \(2001\)](#), and \sum_{xy} is a horizontal sum. The upper 1500m is expanded relative to the deeper ocean, in order to highlight the generally larger surface drifts. 0.05psu contours are drawn to better gauge the magnitude of the drift. Compare to Figure 6 of [Griffies et al. \(2009\)](#) for results from other CORE-NYF simulations.

2.3 Surface ocean properties

We present here three common surface ocean properties considered in climate simulations. Figure 4 shows the bias for the sea surface temperature relative to the the climatology of [Reynolds et al. \(2002\)](#). The model result is taken from a time mean over years 481-500 from the simulations. Figure 5 shows the bias for the sea surface salinity, and Figure 6 shows the bias for the sea surface height. The four simulations share much in common. Indeed, each are much closer to one another than any of the seven simulations shown in [Griffies et al. \(2009\)](#).

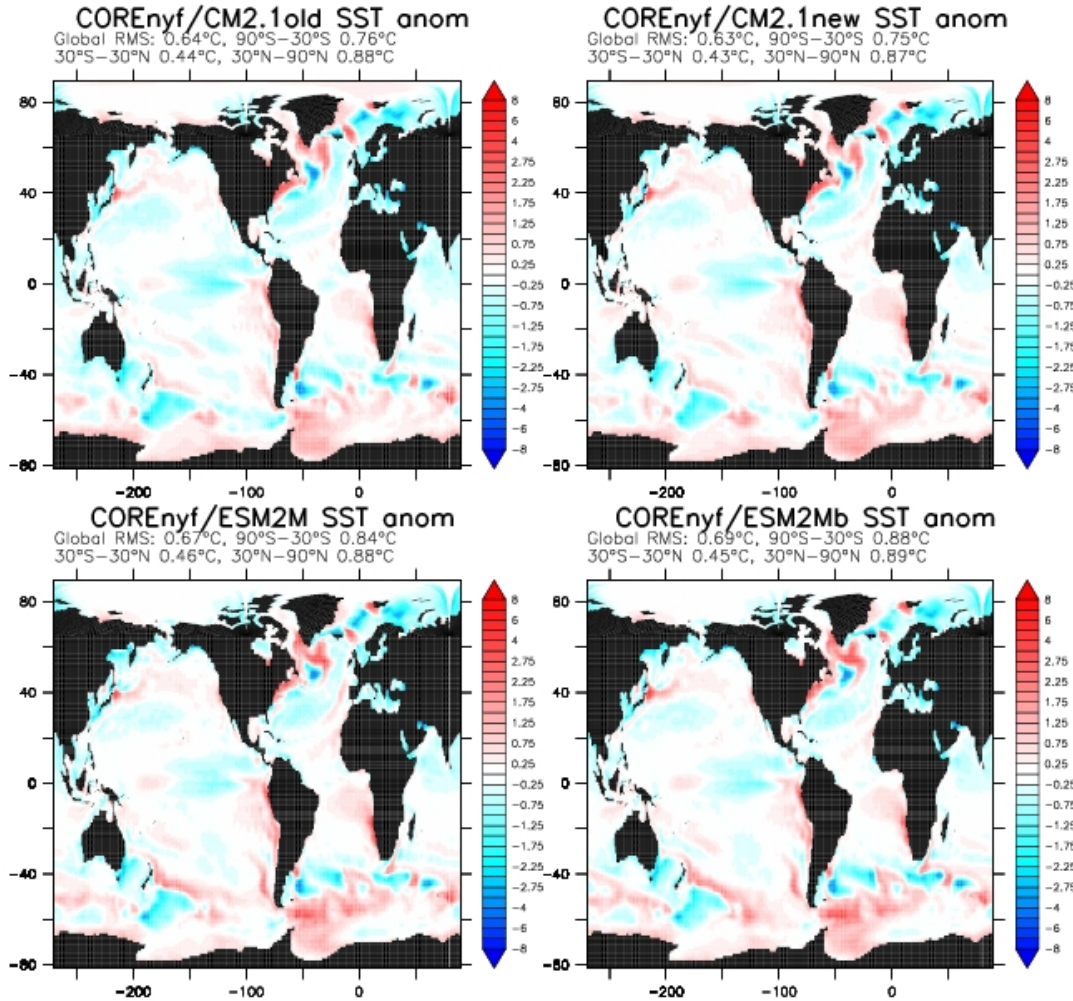


Figure 4: Anomalous sea surface temperature for CORE-NYF simulations, computed as the difference between the climatology of [Reynolds et al. \(2002\)](#) and the time mean for years 481-500 from the simulations. The root-mean-square deviations from the observations are also provided for the global ocean, southern hemisphere middle and high latitudes, tropics, and northern middle and high latitudes. Compare to Figure 7 of [Griffies et al. \(2009\)](#) for results from other CORE-NYF simulations.

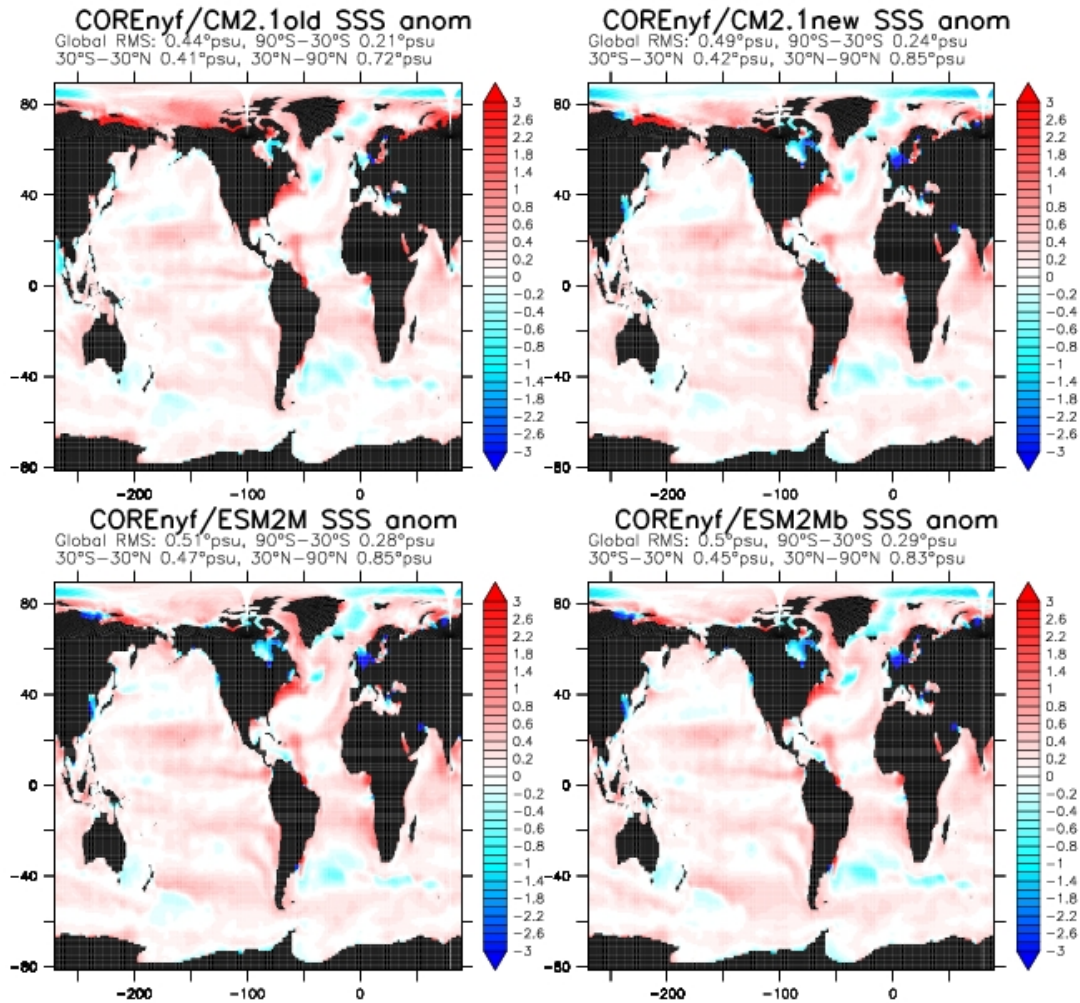


Figure 5: Anomalous sea surface salinity for CORE-NYF simulations, computed as the difference between World Ocean Atlas and the time mean for years 481–500 from the simulations. The root-mean-square deviations from the observations are also provided for the global ocean, southern hemisphere middle and high latitudes, tropics, and northern middle and high latitudes. Compare to Figure 8 of Griffies et al. (2009) for results from other CORE-NYF simulations.

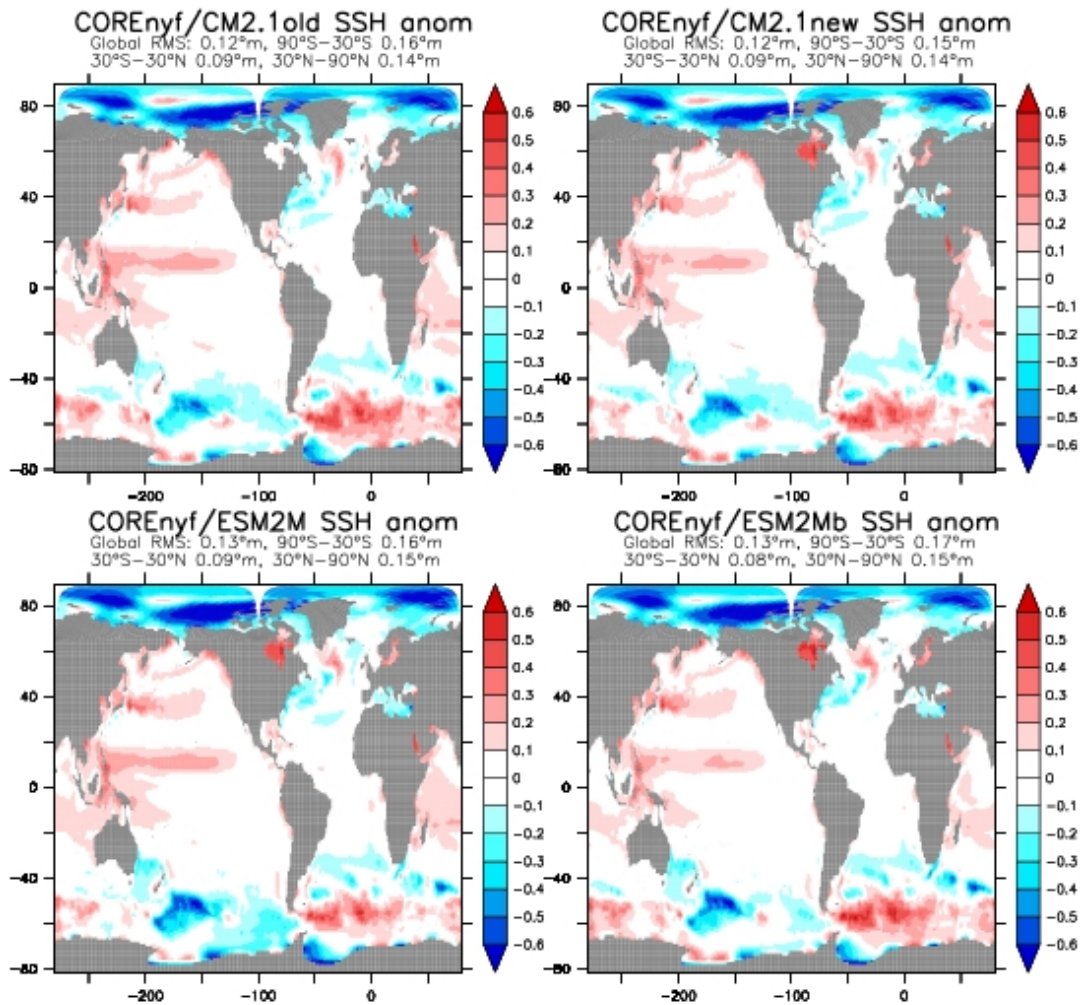


Figure 6: Anomalous sea surface height for CORE-NYF simulations, computed as the difference between analysis from [Maximenko and Niiler \(2005\)](#) and the time mean for years 481–500 from the simulations. Root-mean-square deviations from the observations are also provided for the global ocean, southern hemisphere middle and high latitudes, tropics, and northern middle and high latitudes. Compare to Figure 13 in [Griffies et al. \(2011\)](#) for results from the CM2.1 and CM3 coupled climate models.

2.4 Mixed layer depth

Figure 7 shows the mixed layer depth for the CORE-NYF simulations. The mixed layer depths are based on an interpolation to find the first depth where the difference in buoyancy relative to the surface is greater than 0.0003 m s^{-2} . This approach follows that described in [Levitus \(1982\)](#).

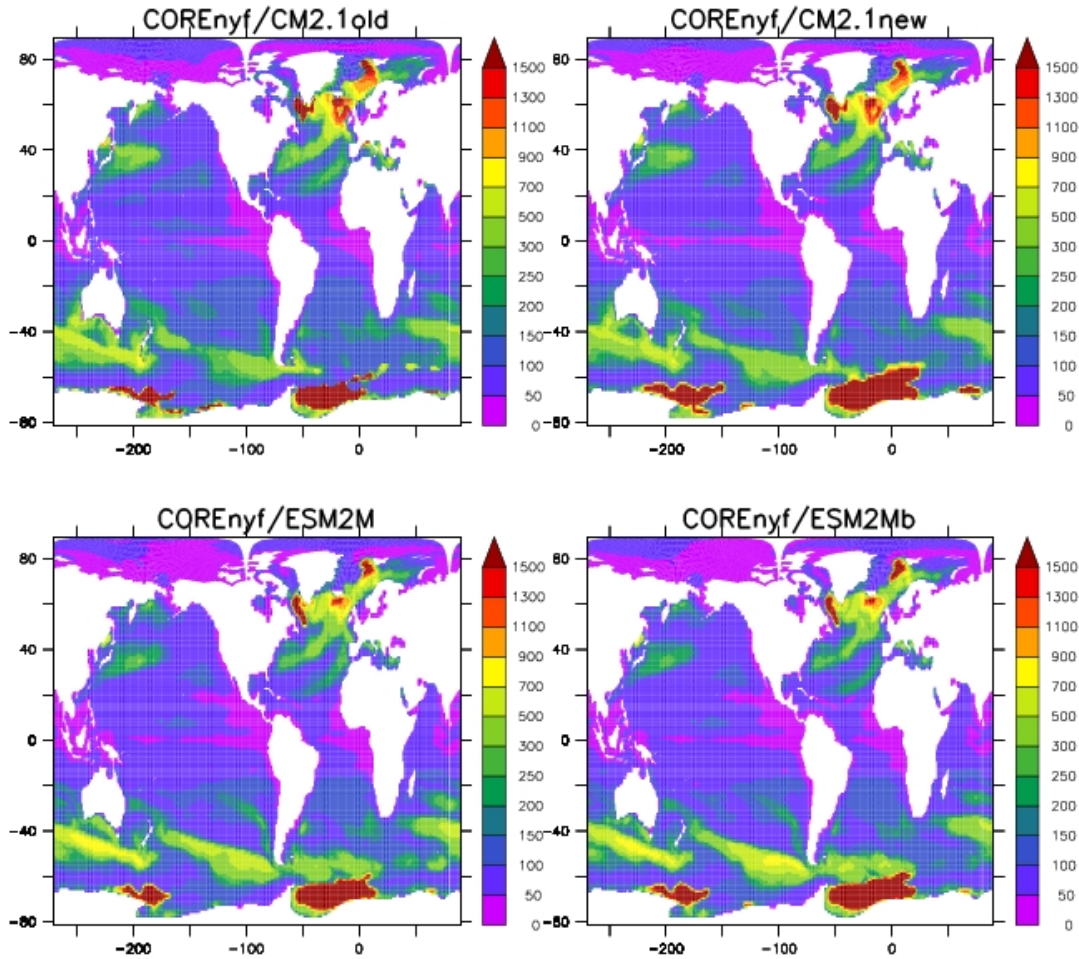


Figure 7: This figure maps the monthly maximum mixed layer depths during simulation years 481-500. That is, for the simulations, at each horizontal grid point, the maximum mixed layer depth is found during years 481-500 for either the monthly averaged mixed layer depth. Compare to Figure 15 of [Griffies et al. \(2009\)](#) for other CORE-NYF simulations.

2.5 Sea ice diagnostics

The simulation of sea ice provides another important surface ocean field that reflects on the integrity of the high latitude fluxes of momentum and buoyancy, with realistic sea ice extent a critical element in the use of a climate model for studying high latitude climate change. Figure 8 shows the bias in the CORE-NYF simulations, and Figure 2.5 shows the climatology seasonal cycle.

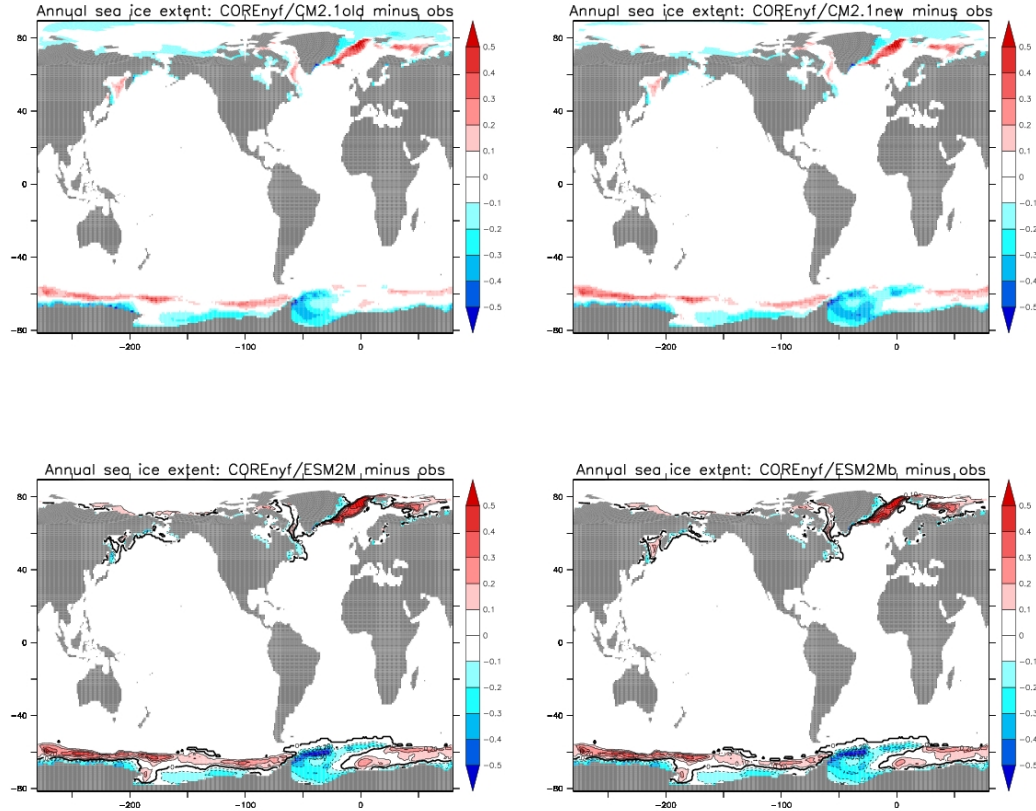


Figure 8: Maps of the annual mean and sea ice extent from the CORE-NYF simulations (averaged over years 481–500) minus a sea ice extent climatology based on observations. The observed ice extent climatology is computed from the monthly sea ice concentrations for years 1981–2000 made available by NCAR and was constructed following the procedure described by [Hurrell et al. \(2008\)](#). Sea ice extent is defined to be unity if the ice concentration is more than 15% for a grid cell area, and zero if there is less ice in a cell. Values between zero and one arise from time averaging. Compare to Figure 9 in [Griffies et al. \(2011\)](#) for results from the CM2.1 and CM3 coupled climate models.

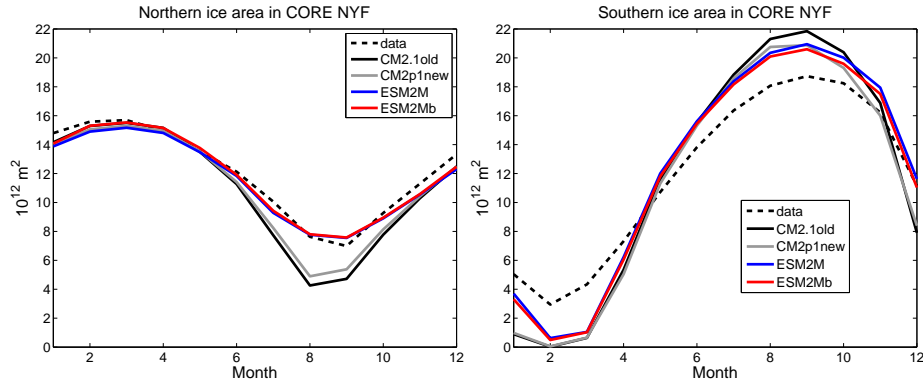


Figure 9: Climatological seasonal cycle of sea ice area computed from the CORE-NYF simulations from years 481-500 in the Northern Hemisphere and Southern Hemisphere. Observational estimates for the seasonal cycle from [Fetterer et al. \(2009\)](#) are shown by the dashed lines. Observational estimates for the annual means from [Cavalieri et al. \(2003\)](#) are roughly $12 \times 10^{12} \text{ m}^2$ for the Northern Hemisphere and $11.5 \times 10^{12} \text{ m}^2$ for the Southern Hemisphere. The annual means for the simulations are for the Northern Hemisphere: CM3 = $12.4 \times 10^{12} \text{ m}^2$, CM2.1 = $13.5 \times 10^{12} \text{ m}^2$, and for the Southern Hemisphere: CM3 = $4.4 \times 10^{12} \text{ m}^2$, CM2.1 = $3.8 \times 10^{12} \text{ m}^2$. Compare to Figure 10 in [Griffies et al. \(2011\)](#) for results from the CM2.1 and CM3 coupled climate models.

2.6 Equatorial Pacific temperature and zonal velocity

Figure 10 shows the temperature along the equator in the Pacific, and Figure 11 shows the same for the zonal velocity.

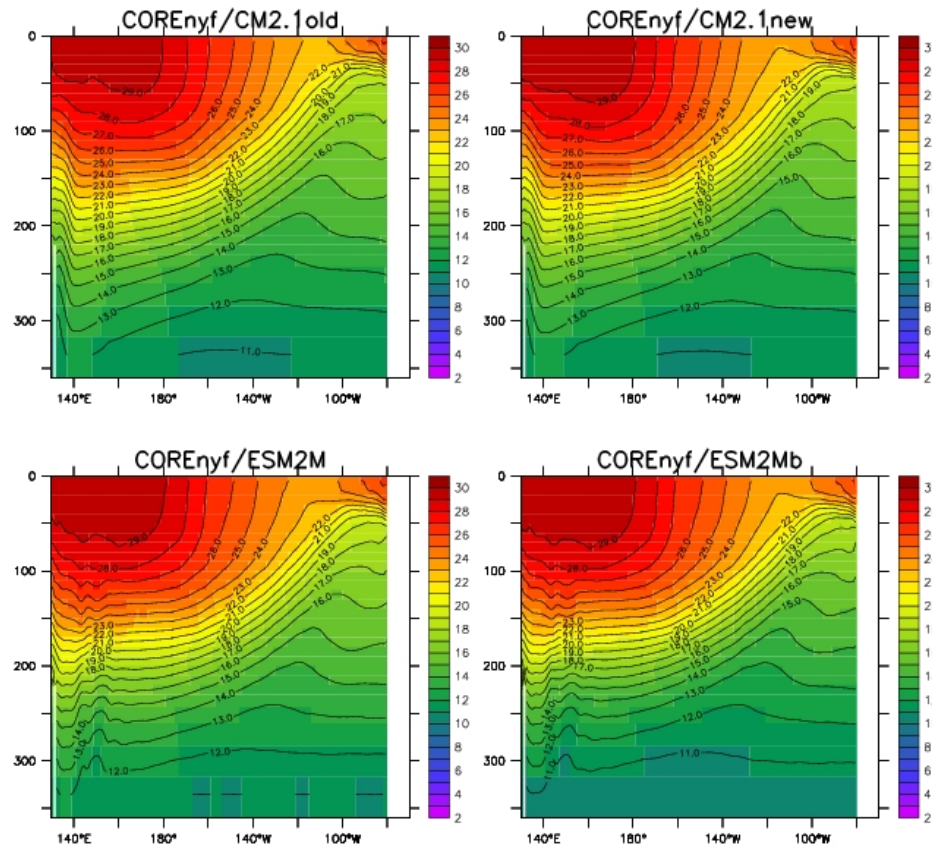


Figure 10: The upper ocean temperature on the equator in the Pacific, with model results from a time mean over years 481-500 of the CORE-NYF simulations. Compare to Figure 13 in [Griffies et al. \(2009\)](#) for results from other CORE-NYF simulations.

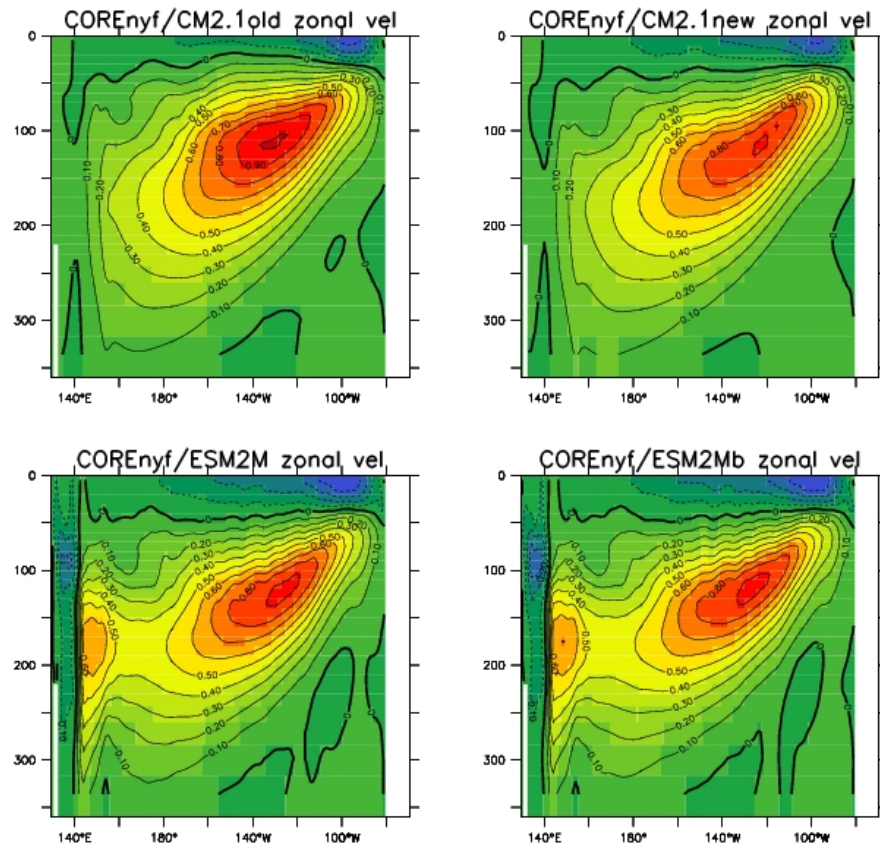


Figure 11: The upper ocean zonal velocity on the equator in the Pacific, with model results from a time mean over years 481-500 of the CORE-NYF simulation. Compare to Figure 14 in Griffies et al. (2009) for results from other CORE-NYF simulations. Note the enhanced structure in the west arises from use of the modified friction in ESM2M and ESM2Mb, relative to that used in CM2.1 (see Section 2.1.3).

2.7 Zonal mean biases for temperature and salinity

Figures 12 and 13 show the zonal mean biases from the CORE-NYF simulations.

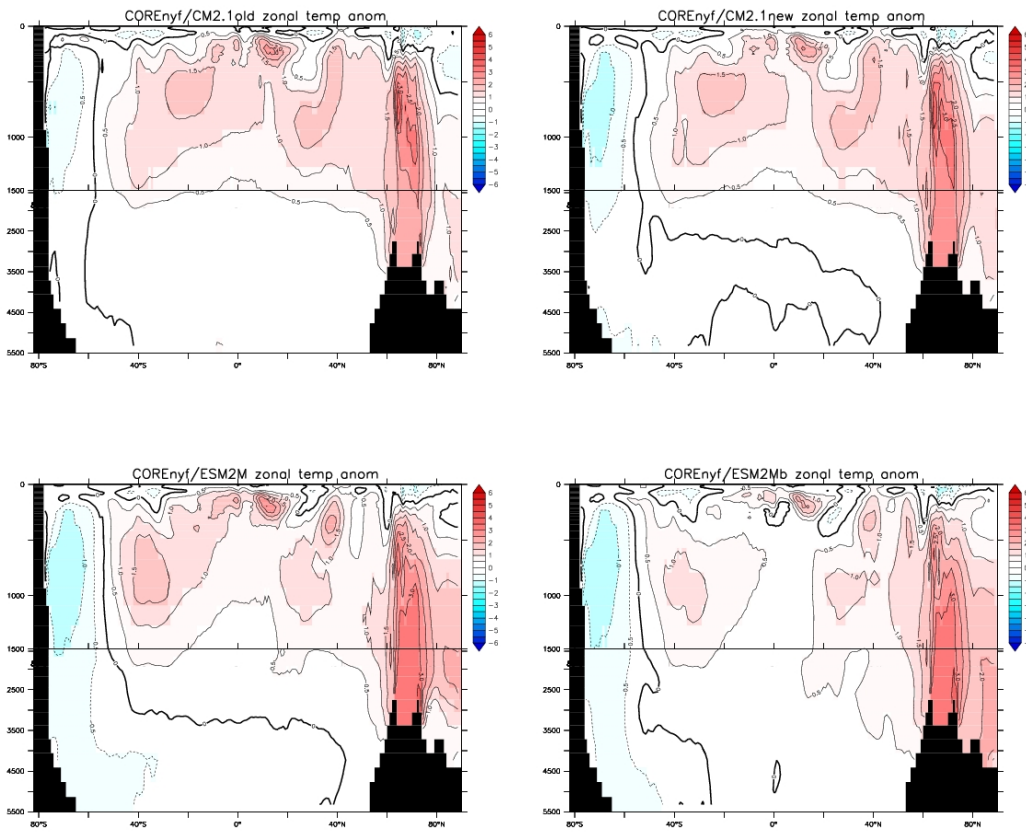


Figure 12: Biases in zonal mean potential temperature, computed as the ensemble mean from the CORE-NYF simulations computed from years 481-500, and differenced from the climatology of Steele et al. (2001). Compare to Figure 16 for other CORE-NYF simulations. Note the significant reduction in zonal mean bias in ESM2Mb within the middle latitude regions.

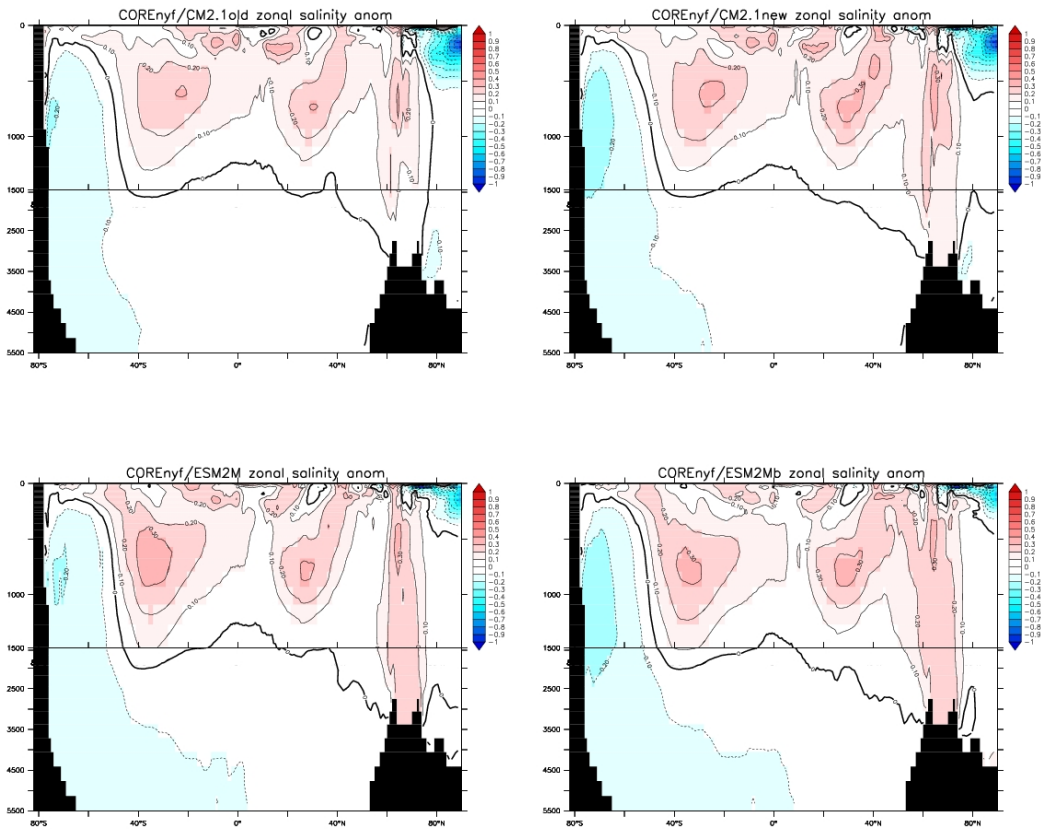


Figure 13: Biases in zonal mean salinity, computed as the ensemble mean from the CORE-NYF simulations computed from years 481-500, and differenced from the climatology of Steele et al. (2001). Compare to Figure 17 for other CORE-NYF simulations.

2.8 Drake Passage and Atlantic time series

Figure 14 shows the time series for the Drake Passage transport and the Atlantic overturning index. Notably, each of the newer simulations show a bit more variability than the original CORE/CM2.1old simulation. It is conjectured that the differences arise from the modifications to the vertical mixing as well as the salinity restoring.

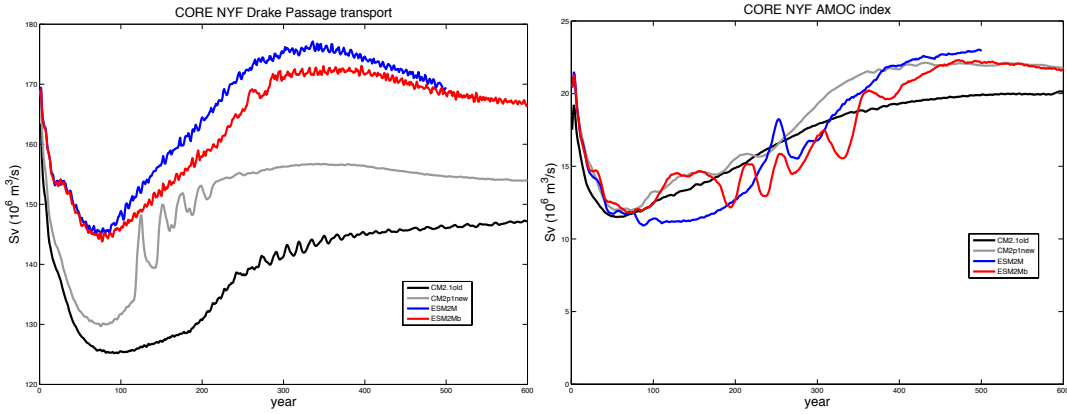


Figure 14: Left panel: Drake Passage transport, which measures the zonal flow through the smallest latitudinal extent of the Antarctic Circumpolar Current (ACC). Drake Passage transport has been measured using various methods, with a low value around 100Sv from [Orsi et al. \(1995\)](#) and high value of 135Sv from [Cunningham et al. \(2003\)](#). [Whitworth \(1983\)](#) and [Whitworth and Peterson \(1985\)](#) give $134 \pm 13\text{Sv}$, with at least some of the models respecting this value. Compare to Figure 18 in [Griffies et al. \(2009\)](#) for other CORE-NYF simulations. Right panel: Time series of the annual mean Atlantic meridional overturning streamfunction index (vertical axis) for model years 1-500 (horizontal axis) in units of $\text{Sv} = 10^6 \text{ m}^3 \text{ sec}^{-1}$. The index is computed as the maximum Atlantic MOC streamfunction at 45°N in the region beneath the wind driven Ekman layer. Note that the GFDL-MOM simulation was extended to 600 years to verify that it was reaching a steady state for the overturning. Observational estimates based on inverse studies from [Ganachaud \(2003\)](#) and [Lumpkin et al. \(2008\)](#) place the transport at 48°N in the range $16 \pm 2 \text{ Sv}$, whereas the inverse study at 42°N by [Ganachaud and Wunsch \(2000\)](#) yields $15 \pm 2 \text{ Sv}$, and [Lumpkin and Speer \(2003\)](#), also at 42°N , yields $13 \pm 2 \text{ Sv}$. Compare to Figure 25 in [Griffies et al. \(2009\)](#) for other CORE-NYF simulations.

2.9 Atlantic and global overturning streamfunction

Figure 15 shows the time mean overturning streamfunction for the CORE-NYF simulations, as a time mean over years 481-500, and Figure 16 shows the same for the World Ocean. Note the increased deep southern transport especially seen in the global overturning. This transport largely arises from changes to the neutral physics scheme implemented in ESM2M relative to CM2.1.

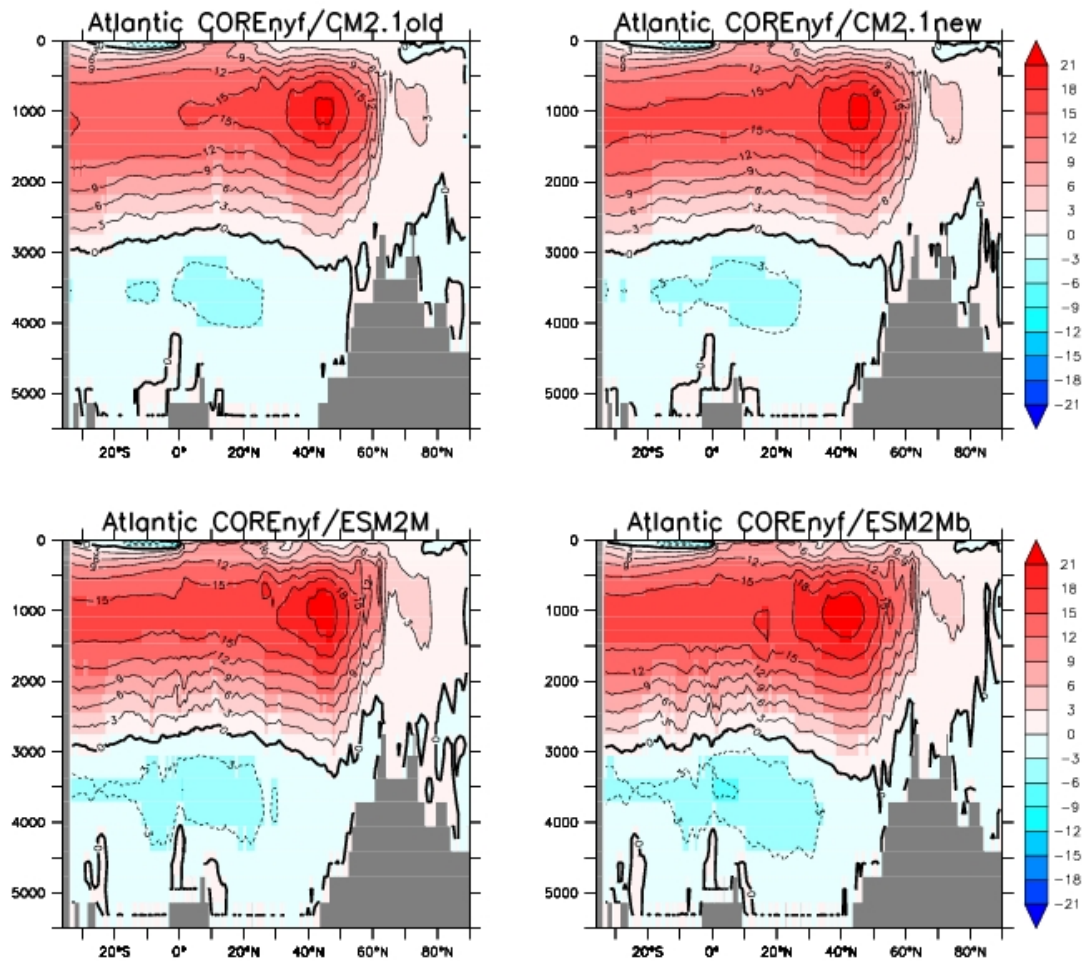


Figure 15: Overturning streamfunction in the Atlantic basin for the CORE-NYF simulations, as computed from a time average over years 481-500. Note the enhanced deep Southern Ocean transport in the CORE/ESM2M and CORE/ESM2Mb simulations. See Figure 24 in Griffies et al. (2009) for comparison to other CORE-NYF simulations.

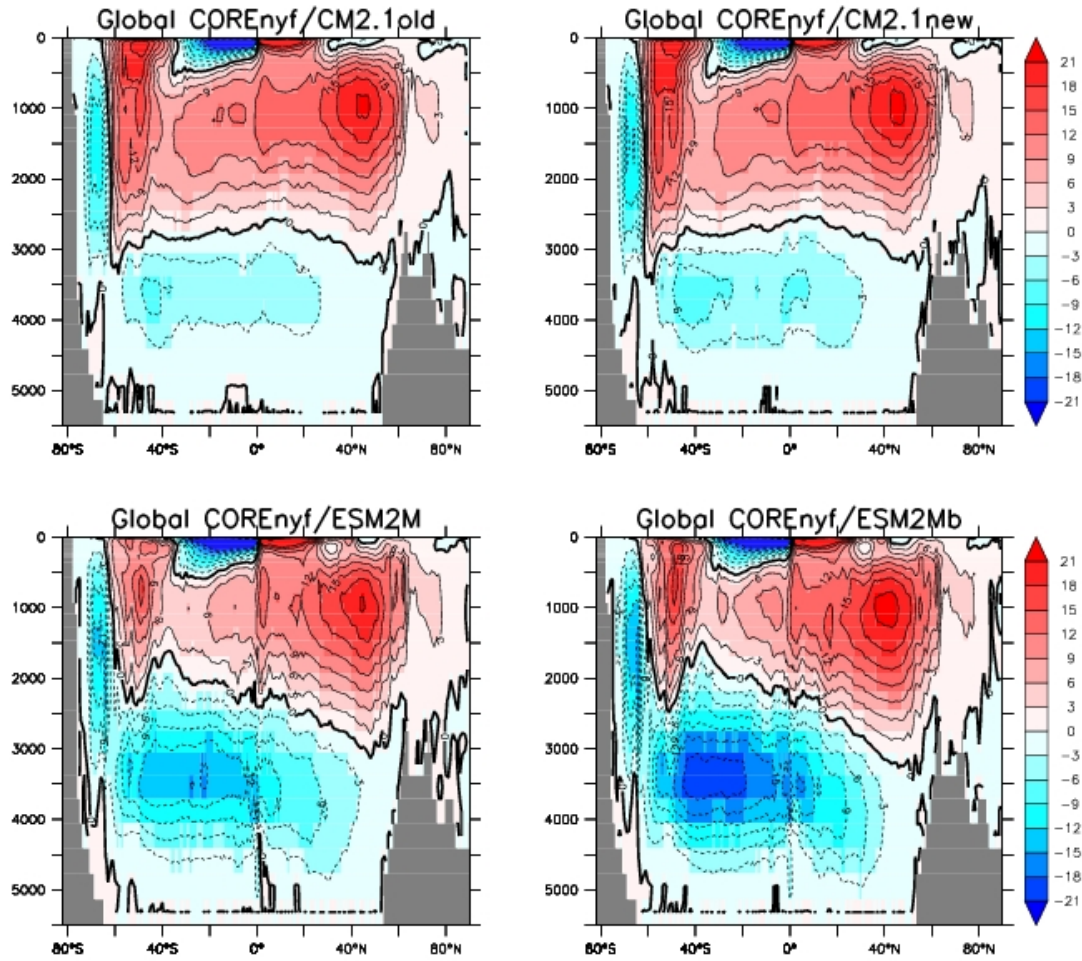


Figure 16: Overturning streamfunction in the World Ocean for the CORE-NYF simulations, as computed from a time average over years 481-500. Note the enhanced overturning in the Southern Ocean for the CORE/ESM2M and CORE/ESM2Mb simulations, as well as the more complete cancellation of the Deacon Cell in these simulations. Both features are associated with the changes to the neutral physics parameterizations detailed in Sections 2.1.3 and 2.1.4. See Figure 24 in Griffies et al. (2009) for comparison to other CORE-NYF simulations.

3 Global ocean-ice-biogeochemistry model

The test case `mom4_om3_ecosystem` consists of a derivative of the realistic global ocean and ice model used for the CORE simulation in Section 2). However, the present test case is somewhat older, and thus a bit obsolete. Nonetheless, it remains a very useful test case to illustrate the ocean biogeochemistry model used for the earth system model ESM2M ([Dunne et al., 2012a,b](#)). That is, this test case enables the GFDL Ocean Biogeochemistry TOPAZ model.

4 Global coupled model CM2.1

The test case `mom4_cm2p1` consists of the same realistic global ocean and ice model used for one of the three CORE-NYF simulations presented in Section 2. In addition, it couples to a realistic atmosphere and land model. This test case is the same configuration used for the GFDL CM2.1 coupled climate model used for the IPCC AR4 assessment, as documented by [Griffies et al. \(2005\)](#), [Gnanadesikan et al. \(2006\)](#), [Delworth et al. \(2006\)](#), [Wittenberg et al. \(2006\)](#), and [Stouffer et al. \(2006a\)](#). This model configuration is being distributed as part of the MOM code release, in hopes that researchers may find it useful both to develop their own coupled climate models, and to make use of the CM2.1 model as it is presently configured.

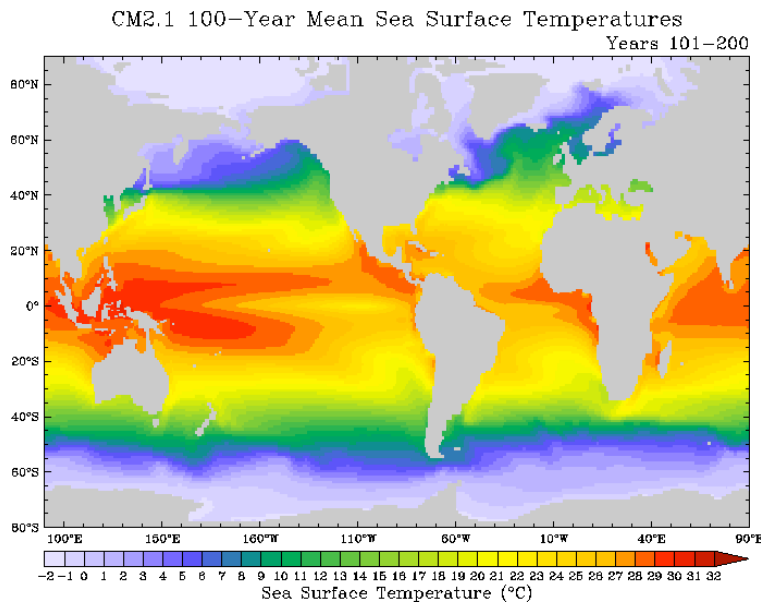


Figure 17: Sea surface temperature climatology from the GFDL coupled climate model CM2.1 as documented by [Griffies et al. \(2005\)](#), [Gnanadesikan et al. \(2006\)](#), [Delworth et al. \(2006\)](#), [Wittenberg et al. \(2006\)](#), and [Stouffer et al. \(2006a\)](#).

5 Global coupled earth system model ESM2M

The test case `mom4_esm2m` consists of the coupled earth system model documented by [Dunne et al. \(2012a,b\)](#). The atmospheric component is very similar to CM2.1 (Section 4), and the ocean component has the same resolution as CM2.1. The main changes to the ocean concern specification of the physical parameterizations. In addition to the physics changes, ESM2M has a full suite of ocean biogeochemistry, land biogeochemistry, and closed carbon cycle. This model is one of two earth system models developed by GFDL for use in the AR5 IPCC climate assessment.

References

- Adcroft, A., Campin, J.-M., 2004. Rescaled height coordinates for accurate representation of free-surface flows in ocean circulation models. *Ocean Modelling* 7, 269–284.
- Adcroft, A., Scott, J. R., Marotzke, J., 2001. Impact of geothermal heating on the global ocean circulation. *Geophysical Research Letters* 28, 1735–1738.
- Black, T. L., 1994. The new NMC mesoscale eta model: description and forecast examples. *Weather and Forecasting* 9, 265–278.
- Bryan, K., Lewis, L. J., 1979. A water mass model of the world ocean. *Journal of Geophysical Research* 84, 2503–2517.
- Cavalieri, D., Parkinson, C., Vinnikov, K., 2003. 30-year satellite record reveals contrasting Arctic and Antarctic decadal variability. *Geophysical Research Letters* 30, doi:10.1029/2003GL018031.
- Conkright, M., Antonov, J., Baranova, O., Boyer, T., Garcia, H., Gelfeld, F., Johnson, D., Locarnini, R., Murphy, P., O'Brien, T., Smolyar, I., Stephens, C., 2002. World Ocean Database 2001, Volume 1: Introduction. NOAA Atlas NESDIS 42, U.S. Government Printing Office 13, NOAA, Washington, D.C., 167 pp.
- Cunningham, S., Alderson, S., King, B., Brandon, M., 2003. Transport and variability of the Antarctic Circumpolar Current in Drake Passage. *Journal of Geophysical Research* 108, Art. 8084.
- Dai, A., Qian, T., Trenberth, K., Milliman, J., 2009. Changes in continental freshwater discharge from 1948–2004. *Journal of Climate* 22, 2773–2791.
- Danabasoglu, G., Large, W. G., Tribbia, J. J., Gent, P. R., Briegleb, B. P., McWilliams, J. C., 2006. Diurnal coupling in the tropical oceans of CCSM3. *Journal of Climate* 19, 2347–2365.
- Danabasoglu, G., McWilliams, J. C., 1995. Sensitivity of the global ocean circulation to parameterizations of mesoscale tracer transports. *Journal of Climate* 8, 2967–2987.
- Delworth, T. L., Broccoli, A. J., Rosati, A., Stouffer, R. J., Balaji, V., Beesley, J. A., Cooke, W. F., Dixon, K. W., Dunne, J., Dunne, K. A., Durachta, J. W., Findell, K. L., Ginoux, P., Gnanadesikan, A., Gordon, C., Griffies, S. M., Gudgel, R., Harrison, M. J., Held, I. M., Hemler, R. S., Horowitz, L. W., Klein, S. A., Knutson, T. R., Kushner, P. J., Langenhorst, A. L., Lee, H.-C., Lin, S., Lu, L., Malyshev, S. L., Milly, P., Ramaswamy, V., Russell, J., Schwarzkopf, M. D., Shevliakova, E., Sirutis, J., Spelman, M., Stern, W. F., Winton, M., Wittenberg, A. T., Wyman, B., Zeng, F., Zhang, R., 2006. GFDL's CM2 global coupled climate models - Part 1: Formulation and simulation characteristics. *Journal of Climate* 19, 643–674.
- Dunne, J. P., John, J. G., Hallberg, R. W., Griffies, S. M., Shevliakova, E. N., Stouffer, R. J., Krasting, J. P., Sentman, L. A., Milly, P. C. D., Malyshev, S. L., Adcroft, A. J., Cooke, W., Dunne, K. A., Harrison, M. J., Levy, H., Samuels, B. L., Spelman, M., Winton, M., Wittenberg, A. T., Phillips, P. J., Zadeh, N., 2012a. GFDLs ESM2 global coupled climate-carbon Earth System Models Part I: Physical formulation and baseline simulation characteristics. *Journal of Climate*, in revision.
- Dunne, J. P., John, J. G., Hallberg, R. W., Griffies, S. M., Shevliakova, E. N., Stouffer, R. J., Krasting, J. P., Sentman, L. A., Milly, P. C. D., Malyshev, S. L., Adcroft, A. J., Cooke, W., Dunne, K. A., Harrison, M. J., Levy, H., Wittenberg, A., Phillips, P., Zadeh, N., 2012b. GFDLs ESM2 global coupled climate-carbon Earth System Models Part II: Carbon system formulation and baseline simulation characteristics. *Journal of Climate*, submitted.
- Farneti, R., Delworth, T., Rosati, A., Griffies, S. M., Zeng, F., 2010. The role of mesoscale eddies in the rectification of the Southern Ocean response to climate change. *Journal of Physical Oceanography* 40, 1539–1557.
- Farneti, R., Gent, P., 2011. The effects of the eddy-induced advection coefficient in a coarse-resolution coupled climate model. *Ocean Modelling*, doi:10.1016/j.ocemod.2011.02.005.

- Ferrari, R., Griffies, S. M., Nurser, A. J. G., Vallis, G. K., 2010. A boundary-value problem for the parameterized mesoscale eddy transport. *Ocean Modelling* 32, 143–156.
- Fetterer, F., Knowles, K., Meier, W., Savoie, M., 2009. Sea ice index. Tech. rep., National Snow and Ice Data Center, Boulder, USA.
- Fox-Kemper, B., Danabasoglu, G., Ferrari, R., Griffies, S. M., Hallberg, R. W., Holland, M., Peacock, S., Samuels, B., 2011. Parameterization of mixed layer eddies. III: Global implementation and impact on ocean climate simulations. *Ocean Modelling* 39, 61–78.
- Fox-Kemper, B., Ferrari, R., Hallberg, R., 2008. Parameterization of mixed layer eddies. I: Theory and diagnosis. *Journal of Physical Oceanography* 38, 1145–1165.
- Ganachaud, A., 2003. Large-scale mass transports, water mass formation, and diffusivities estimated from World Ocean Circulation Experiment (WOCE) hydrographic data. *Journal of Geophysical Research* 108, doi:10.1029/2002JC001565.
- Ganachaud, A., Wunsch, C., 2000. Improved estimates of global ocean circulation, heat transport and mixing from hydrographic data. *Nature* 408, 453–456.
- Gent, P. R., McWilliams, J. C., 1990. Isopycnal mixing in ocean circulation models. *Journal of Physical Oceanography* 20, 150–155.
- Gent, P. R., Willebrand, J., McDougall, T. J., McWilliams, J. C., 1995. Parameterizing eddy-induced tracer transports in ocean circulation models. *Journal of Physical Oceanography* 25, 463–474.
- Gnanadesikan, A., Dixon, K. W., Griffies, S. M., Balaji, V., Beesley, J. A., Cooke, W. F., Delworth, T. L., Gerdes, R., Harrison, M. J., Held, I. M., Hurlin, W. J., Lee, H.-C., Liang, Z., Nong, G., Pacanowski, R. C., Rosati, A., Russell, J., Samuels, B. L., Song, S. M., Spelman, M. J., Stouffer, R. J., Sweeney, C. O., Vecchi, G., Winton, M., Wittenberg, A. T., Zeng, F., Zhang, R., 2006. GFDL's CM2 global coupled climate models-Part 2: The baseline ocean simulation. *Journal of Climate* 19, 675–697.
- Griffies, S. M., 1998. The Gent-McWilliams skew-flux. *Journal of Physical Oceanography* 28, 831–841.
- Griffies, S. M., Biastoch, A., Böning, C. W., Bryan, F., Chassignet, E., England, M., Gerdes, R., Haak, H., Hallberg, R. W., Hazeleger, W., Jungclaus, J., Large, W. G., Madec, G., Samuels, B. L., Scheinert, M., Gupta, A. S., Severijns, C. A., Simmons, H. L., Treguier, A. M., Winton, M., Yeager, S., Yin, J., 2009. Coordinated Ocean-ice Reference Experiments (COREs). *Ocean Modelling* 26, 1–46.
- Griffies, S. M., Böning, C. W., Bryan, F. O., Chassignet, E. P., Gerdes, R., Hasumi, H., Hirst, A., Treguier, A.-M., Webb, D., 2000. Developments in ocean climate modelling. *Ocean Modelling* 2, 123–192.
- Griffies, S. M., Gnanadesikan, A., Dixon, K. W., Dunne, J. P., Gerdes, R., Harrison, M. J., Rosati, A., Russell, J., Samuels, B. L., Spelman, M. J., Winton, M., Zhang, R., 2005. Formulation of an ocean model for global climate simulations. *Ocean Science* 1, 45–79.
- Griffies, S. M., Gnanadesikan, A., Pacanowski, R. C., Larichev, V., Dukowicz, J. K., Smith, R. D., 1998. Isoneutral diffusion in a z-coordinate ocean model. *Journal of Physical Oceanography* 28, 805–830.
- Griffies, S. M., Hallberg, R. W., 2000. Biharmonic friction with a Smagorinsky viscosity for use in large-scale eddy-permitting ocean models. *Monthly Weather Review* 128, 2935–2946.
- Griffies, S. M., Winton, M., Donner, L. J., Downes, S. M., Farneti, R., Gnanadesikan, A., Horowitz, L. W., Hurlin, W. J., Lee, H.-C., Liang, Z., Palter, J. B., Samuels, B. L., Wittenberg, A. T., Wyman, B. L., Yin, J., Zadeh, N. T., 2011. GFDL's CM3 coupled climate model: Characteristics of the ocean and sea ice simulations. *Journal of Climate* 24, 3520–3544.
- Hurrell, J., Hack, J., Shea, D., Caron, J., Rosinski, J., 2008. A new sea surface temperature and sea ice boundary data set for the Community Atmosphere Model. *Journal of Climate* 21, 5145–5153.

- Kopp, R. E., Mitrovica, J. X., Griffies, S. M., Yin, J., Hay, C. C., Stouffer, R. J., 2010. The impact of Greenland melt on regional sea level: a preliminary comparison of dynamic and static equilibrium effects. *Climatic Change Letters* 103, 619–625.
- Large, W., McWilliams, J., Doney, S., 1994. Oceanic vertical mixing: a review and a model with a nonlocal boundary layer parameterization. *Reviews of Geophysics* 32, 363–403.
- Large, W., Yeager, S., 2004. Diurnal to decadal global forcing for ocean and sea-ice models: the data sets and flux climatologies. NCAR Technical Note: NCAR/TN-460+STR. CGD Division of the National Center for Atmospheric Research.
- Large, W. G., Danabasoglu, G., McWilliams, J. C., Gent, P. R., Bryan, F. O., 2001. Equatorial circulation of a global ocean climate model with anisotropic horizontal viscosity. *Journal of Physical Oceanography* 31, 518–536.
- Large, W. G., Yeager, S., 2009. The global climatology of an interannually varying air-sea flux data set. *Climate Dynamics* 33, 341–364.
- Lee, H.-C., Rosati, A., Spelman, M., 2006. Barotropic tidal mixing effects in a coupled climate model: Oceanic conditions in the northern Atlantic. *Ocean Modelling* 3-4, 464–477.
- Levitus, S., 1982. Climatological atlas of the world ocean. U.S. Government Printing Office 13, NOAA, Washington, D.C., 163 pp.
- Lumpkin, R., Speer, K., 2003. Large-scale vertical and horizontal circulation in the North Atlantic Ocean. *Journal of Physical Oceanography* 33, 1902–1920.
- Lumpkin, R., Speer, K., Koltermann, K., 2008. Transport across 48°N in the Atlantic Ocean. *Journal of Physical Oceanography* 38, 733–752.
- Manizza, M., Le Quere, C., Watson, A., Buitenhuis, E., 2005. Bio-optical feedbacks among phytoplankton, upper ocean physics and sea-ice in a global model. *Geophysical Research Letters* 32, doi:10.1029/2004GL020778.
- Marshall, J., Hill, C., Perelman, L., Adcroft, A., 1997. Hydrostatic, quasi-hydrostatic, and nonhydrostatic ocean modeling. *Journal of Geophysical Research* 102, 5733–5752.
- Maximenko, N., Niiler, P., 2005. Hybrid decade-mean global sea level with mesoscale resolution. In: Saxena, N. (Ed.), *Recent Advances in Marine Science and Technology 2004*. PACON International, Honolulu, pp. 55–59.
- Morel, A., Antoine, D., 1994. Heating rate within the upper ocean in relation to its bio-optical state. *Journal of Physical Oceanography* 24, 1652–1665.
- Orsi, A., Whitworth, T., Nowlin, W., 1995. On the meridional extent and fronts of the antarctic circumpolar current. *Deep-Sea Research* 42A, 641–673.
- Perovich, D., Grenfell, T. C., Light, B., Hobbs, P. V., 2002. Seasonal evolution of the albedo of multiyear Arctic sea ice. *Journal of Geophysical Research* 107(C10), 8044.
- Rahmstorf, S., 1993. A fast and complete convection scheme for ocean models. *Ocean Modelling* 101, 9–11.
- Reynolds, R. W., Rayner, N., Smith, T. M., Stokes, D., Wang, W., 2002. An improved *in situ* and satellite SST analysis for climate. *Journal of Climate* 15, 1609–1625.
- Simmons, H. L., Jayne, S. R., St.Laurent, L. C., Weaver, A. J., 2004. Tidally driven mixing in a numerical model of the ocean general circulation. *Ocean Modelling* 6, 245–263.
- Stacey, M. W., Pond, S., Nowak, Z. P., 1995. A numerical model of the circulation in Knight Inlet, British Columbia, Canada. *Journal of Physical Oceanography* 25, 1037–1062.

- Steele, M., Morfley, R., Ermold, W., 2001. PHC: A global ocean hydrography with a high-quality Arctic Ocean. *Journal of Climate* 14, 2079–2087.
- Stouffer, R. J., Broccoli, A., Delworth, T., Dixon, K., Gudgel, R., Held, I., Hemler, R., Knutson, T., Lee, H.-C., Schwarzkopf, M., Soden, B., Spelman, M., Winton, M., Zeng, F., 2006a. GFDL's CM2 global coupled climate models: Part 4: idealized climate response. *Journal of Climate* 19, 723–740.
- Stouffer, R. J., Dixon, K., Spelman, M., Hurlin, W., Yin, J., Gregory, J., Weaver, A., Eby, M., Flato, G., Robitaille, D., Hasumi, H., Oka, A., Hu, A., Jungclaus, J., Kamenkovich, I., Levermann, A., Montoya, M., Murakami, S., Nawrath, S., Peltier, W., Vettoretti, G., Sokolov, A., Weber, S., 2006b. Investigating the causes of the response of the thermohaline circulation to past and future climate changes. *Journal of Climate* 19, 1365–1387.
- Sweeney, C., Gnanadesikan, A., Griffies, S. M., Harrison, M., Rosati, A., Samuels, B., 2005. Impacts of shortwave penetration depth on large-scale ocean circulation and heat transport. *Journal of Physical Oceanography* 35, 1103–1119.
- Whitworth, T., 1983. Monitoring the transport of the Antarctic Circumpolar Current at Drake Passage. *Journal of Physical Oceanography* 13, 2045–2057.
- Whitworth, T., Peterson, R., 1985. Volume transport of the antarctic circumpolar current from bottom pressure measurements. *Journal of Physical Oceanography* 15, 810–816.
- Winton, M., 2000. A reformulated three-layer sea ice model. *Journal of Atmospheric and Oceanic Technology* 17, 525–531.
- Wittenberg, A., Rosati, A., Lau, G., Poshay, J., 2006. GFDL's CM2 global coupled climate models - Part 3: Tropical Pacific climate and ENSO. *Journal of Climate* 19, 698–722.
- Yin, J., Stouffer, R., Spelman, M. J., Griffies, S. M., 2010. Evaluating the uncertainty induced by the virtual salt flux assumption in climate simulations and future projections. *Journal of Climate* 23, 80–96.